Static and fatigue performance of stud shear connector in steel fiber reinforced concrete

Chen Xu [*1], Qingtian Su [1a] and Hiroshi Masuya [2b]

[1] *Department of Bridge Engineering, College of Civil Engineering, Tongji University, 1239 Siping Rd, Shanghai, China*
[2] *Department of Environmental Design, Institute of Science and Engineering, Kanazawa University, Kakumamachi, Kanazawa, Japan*

Abstract. The stud is one of the most frequently used shear connectors which are important to the steel-concrete composite action. The static and fatigue behavior of stud in the steel fiber reinforced concrete (SFRC) were particularly concerned in this study through the push-out tests and analysis. It was for the purpose of investigating and explaining a tendency proposed by the current existing researches that the SFRC may ameliorate the shear connector's mechanical performance, and thus contributing to the corresponding design practice. There were 20 test specimens in the tests and 8 models in the analysis. According to the test and analysis results, the SFRC had an obvious effect of restraining the concrete damage and improving the stud static performance when the compressive strength of the host concrete was relatively low. As to the fatigue aspect, the steel fibers in concrete also tended to improve the stud fatigue life, and the favorable tensile performance of SFRC may be the main reason. But such effect was found to vary with the fatigue load range. Moreover, the static and fatigue test results were compared with several design codes. Particularly, the fatigue life estimation of Eurocode 4 appeared to be less conservative than that of AASHTO, and to have higher safety redundancy than that of JSCE hybrid structure guideline.

Keywords: stud shear connector; steel fiber reinforced concrete (SFRC); stud mechanical performance; fatigue life

1. Introduction

The shear connector's mechanical performance is important to the steel-concrete composite action. And the stud is one of the most frequently used shear connectors. There has been a long period of researching on a variety of effects on the stud connector, such as the concrete cracks (Gao *et al.* 2016, Xu and Sugiura 2013), the arrangement effect (Lin *et al.* 2015, Shim *et al.* 2008), the stud dimension (Nguyen and Machacek 2016, Badie *et al.* 2011), and the loading effect (Ju and Zeng 2015), etc. The effect of steel fiber reinforced concrete (SFRC) has also been concerned while the detail, especially on the stud fatigue aspect, is not enough. In fact, the SFRC has always been considered to resist the tensile concrete cracks in the negative flexural region of a continuous composite girder in light of its favorable tensile performance (Lin *et al.* 2014). The 4-span 189 m-long Monobekawa continuous composite railway bridge in the ASA line of Japan is a typical example of using the steel fibers (Φ0.6×30 mm, vol. 1.5%) to resist the concrete cracks in the negative flexural region (Hosaka *et al.* 2000). On the other hand, the SFRC was also used for rehabilitating the fatigue damage on the steel decks. The Public Works Research Institute (2009) presented the real engineering examples and the tentative guidelines for the

steel deck rehabilitation by using SFRC. The bond and stud connectors were considered to connect the SFRC slab and the steel deck.

In 2002, Lam and Nip (2002) carried out 6 horizontal static push-off tests on the 19 mm shank diameter stud and reported that the 2.0% vol. steel fibers in concrete improved the stud strength and slip ductility. Later, Mirza and Uy (2009) carried out 6 push-out tests and related FEM analysis with the same stud diameter. It showed that the SFRC effect on the stud shear stiffness and strength was obvious when the volume percentages of the steel fibers were 0.3% or 0.6%. The concrete compressive strength in the test was around 33.6 MPa, and the tensile strength was not specified. Moreover, Cui and Nakashima (2012) and Luo *et al.* (2016) investigated the static behavior of stud connectors in SFRCC (steel fiber reinforced cementitious composites) for the purpose of developing a kind of weld-free beam-column connection. It was reported that the shear transfer from the stud to the SFRCC could be improved by the 6% vol. steel fibers. As to other connectors, Choi *et al.* (2011) showed the favorable effect of steel fibers in the lightweight concrete on the perfobond shear stiffness and strength. Generally, these researches indicated that the SFRC might have the possibility to ameliorate the shear connector's mechanical performance. However, the details of the static and fatigue performance of stud in SFRC remain unclear. In this case, a series of static and cyclic push-out tests and analysis were carried out to investigate the effect of SFRC on the stud performance which included the failure mode, stiffness and strength, fatigue life, slip feature, etc.

∗Corresponding author, Associate Professor,
  E-mail: xuchenprc@tongji.edu.cn
[a] Professor
[b] Professor

2. Experimental works

2.1 Test specimens

There were 20 push-out test specimens in this study, which were categorized into two types (Type A and Type B) in terms of the stud dimension. The nominal stud shank diameter and height in Type A specimen were 13 mm and 80 mm, and the corresponding values in Type B specimens were 19 mm and 150 mm. The specimen dimensions were shown in Fig. 1. Each of the specimens contained the twin concrete blocks, the steel flanges and the studs. The transverse stud spacing was 100 mm. The studs were welded on steel flanges. The approximate minimums of the stud welding toe h, the welding height v, the welding thickness t in the Type A specimens were respectively around 3.2 mm, 3.8 mm, and 3.2 mm. And the corresponding ones in the Type B specimens were 4.4 mm, 4.5 mm and 4.4 mm. The embedded reinforcement diameter was 10 mm. In addition, the steel-concrete interlayer bonding and fiction were removed as much as possible by greasing oil on the interlayer surfaces of steel flanges.

The specimen details including the concrete type (Normal and SFRC) and the load feature (static and cyclic) were listed in Table 1. There were three kinds of steel fiber volume percentages (0%, 1.0% and 1.5%) in SFRC. The steel fibers as shown in Fig. 2 were with the end hooks, and the fiber length and diameter were 30 mm and 0.62 mm. The steel fiber's nominal ultimate tensile strength was 1080 MPa. Fig. 3 shows the steel fibers mixed with the fresh concrete. The compressive strength of SFRC and normal concrete in the tests was designed to be 40 MPa. As to the cyclic push-out tests in particular, there were four kinds of cyclic loads applied on the specimens. The cyclic load

range (ΔP) varied from approximate 36% to 30% of P_u, where P_u was the static shear strength of stud the in normal concrete. The cyclic mean load was designed to be 30% of P_u. The corresponding stud shear stress range ($\Delta \tau = \Delta P / A_s$, A_s was the sectional area of stud shank) was also listed in Table 1.

2.2 Material properties

The uniaxial compression and splitting tension tests on

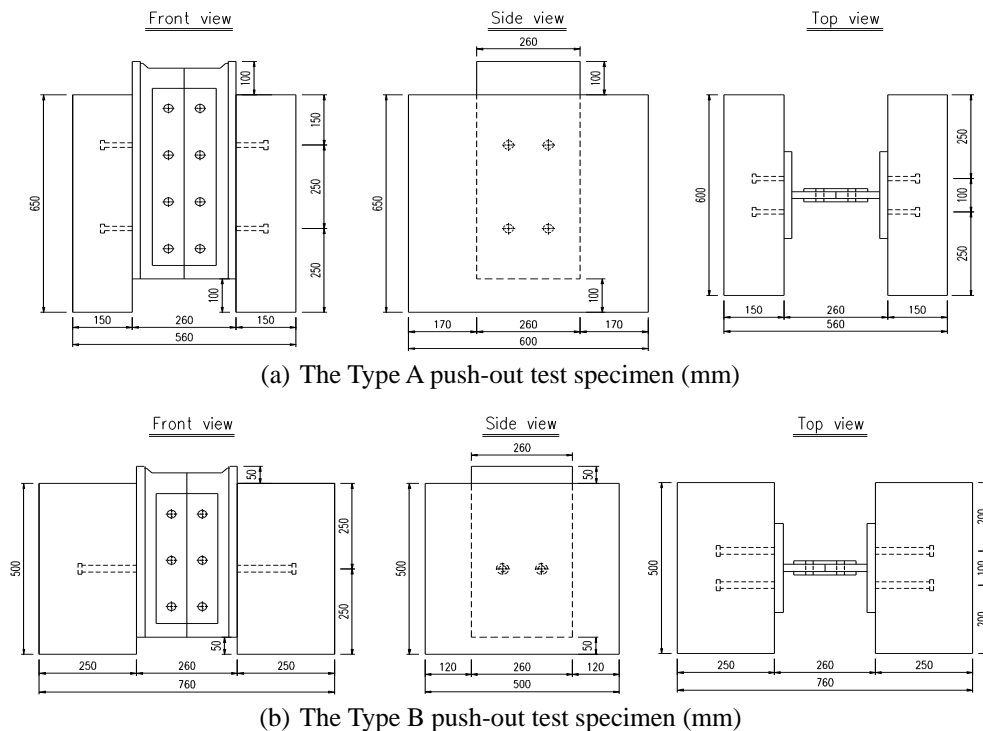Fig. 2 Steel fibers

Fig. 3 Fresh SFRC

(a) The Type A push-out test specimen (mm)

(b) The Type B push-out test specimen (mm)

Fig. 1 Layout of the Type A and Type B push-out test specimens (mm)

Table 1 The concrete material properties (MPa)

Specimens	Test pattern	Concrete material	Load mean (P_u)	Load range (P_u)	Stress range (MPa)
ASN1		Normal			
ASF1		SFRC (1.0% Vol.)			
ASF2		SFRC (0.5% Vol.)			
BSN1	Static	Normal	N/A		
BSN2					
BSF1		SFRC (1.5% Vol.)			
BSF2					
BSF3		SFRC (1.0% Vol.)			
BSF4					
ACN1		Normal		0.32	180
ACF1		SFRC (1.0% Vol.)		0.30	170
ACF2				0.32	180
ACF3		SFRC (0.5% Vol.)		0.30	170
BCN1		Normal		0.36	213
BCN2	Cyclic		0.30	0.33	195
BCN3				0.30	180
BCF1		SFRC (1.5% Vol.)		0.36	213
BCF2				0.33	195
BCF3				0.30	180
BCF4		SFRC (1.0% Vol.)		0.30	180

*P_u: the static shear strength of stud in the Type A or Type B specimen with the normal concrete

Table 2 The concrete material properties (MPa)

Concrete	Curing age	A series specimens			B series specimens		
		f_t	f_c	E	f_t	f_c	E
Normal	7 days	2.3	29.8	30366	2.7	27.4	24500
	28 days	2.4	43.9	32708	3.0	39.8	31500
SFRC (A: 1.0%, B: 1.5%)	7 days	2.7	28.1	26498	2.8	25.5	27700
	28 days	3.4	36.4	29700	3.2	28.5	30500
SFRC (A: 0.5%, B: 1.0%)	7 days	2.5	27.8	31498	3.1	34.1	34156
	28 days	-	-	-	3.5	39.2	35759
	302 days	4.1	45.8	34659	-	-	-

*Note − f_t: tensile strength; f_c: compressive strength; E: modulus

the concrete were carried out twice at least after 7 days and 28 days curing age. Due to the fatigue test schedule, there were additional concrete material tests for the Type A fatigue test specimens after 302 days curing age. The compression test specimens were cylinders, 200 mm high with a diameter of 100 mm. The splitting tension test specimens were cylinders as well, 150 mm high with a diameter of 150 mm. The material modulus was also measured. The results were listed in Table 2. It has to be mentioned here that the tested 28-days compressive strength of SFRC (1.5% vol.) was obviously lower than 40 MPa, which was not as expected. The unskillful casting operation of steel fiber reinforced concrete was the reason. The slump of the SFRC (1.5% vol.) for casting was 11.0 cm. Even though the steel fibers were confirmed distributed evenly in concrete, the fresh concrete might not experience enough vibration during casting. Nevertheless, the modulus and tensile strength were still rational. Moreover, the tested yield and ultimate stress of stud were 380.4 and 455.5 MPa, respectively.

2.3 Load setup and sensors

Fig. 4 presents the push-load setup based on the JSSC

(JSSC 1996). A ball seat was placed under the vertical load jack for maintaining the vertical load direction. A load cell and a distribution girder were placed between the specimen and the ball seat respectively for monitoring the exact push load supported by the specimen and the load uniformity. Meanwhile, a piece of sand was placed between the specimen bottom and bearing steel plate to avoid the force concentration.
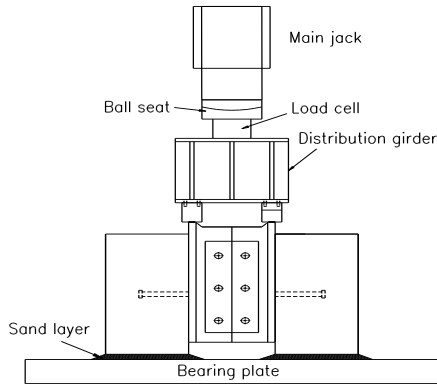
Fig. 5(a) shows the static load procedure. A pre-load step was introduced before the formal load application, in which the load maximum was set to 60 kN, less than 10% of the estimated ultimate load. The following formal load procedure contained two steps. In step1, the load was applied on a specimen monotonically until 200 kN, larger than one third of the estimated ultimate load. This was for checking the stiffness and the corresponding residual slip in
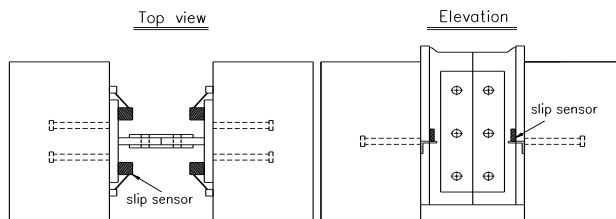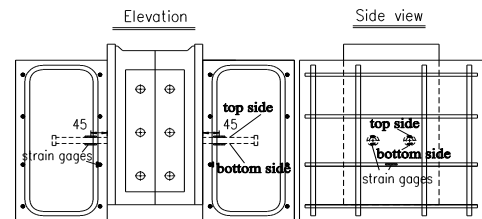

Fig. 4 Load setup
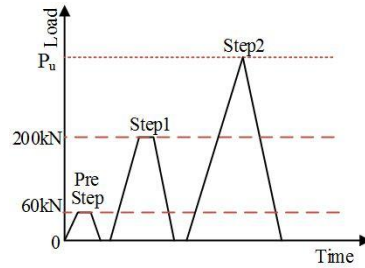
(a) Static test
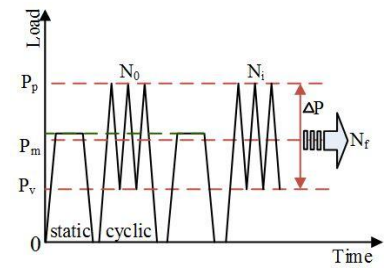
(b) Fatigue test

Fig. 5 Static and cyclic load procedure

P_p, P_v and P_m are respectively the cyclic load peak, valley and mean; ΔP is the cyclic load range;
P_u: the static shear strength of stud in the Type A or Type B specimen with the normal concrete
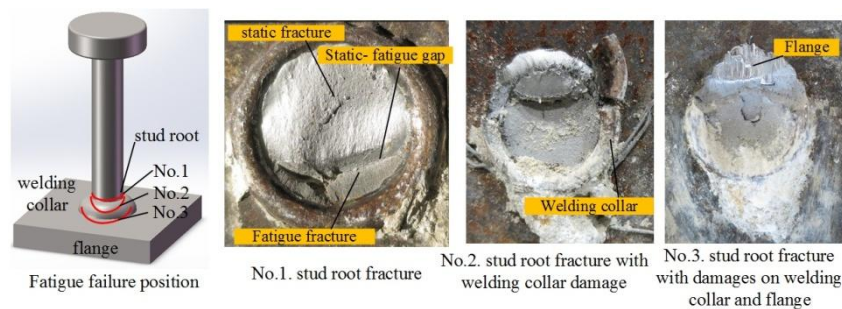

(a) Slip sensors

(b) Uniaxial strain gauges

Fig. 6 Sensors and gauges

Concrete damage (BSN1)   SFRC damage (BSF3)   Stud root fracture (BSF1)

(a) Static push-out failure (stud fracture with local concrete or SFRC damage)

Fatigue failure position   No.1. stud root fracture   No.2. stud root fracture with welding collar damage   No.3. stud root fracture with damages on welding collar and flange

(b) Stud fracture modes in the fatigue push-out tests

Fig. 7 Failure modes (images by Chen Xu)

the test process. In step2, the load was applied monotonically until failure.

Fig. 5(b) shows the cyclic load procedure, in which the P_p, P_v and P_m were respectively the cyclic load peak, valley and mean. The fatigue load frequency was around 2~3 Hz. The stiffness variation was measured during the fatigue test by applying a static load up to $P_u/3$ at certain numbers of load cycles. Finally, the fatigue lives of stud corresponding to the certain kinds of cyclic load patterns were derived.

Fig. 6(a) shows 4 slip sensors symmetrically mounted on a specimen. Meanwhile, as shown in Fig. 6(b), a pair of uniaxial strain gauges were mounted at the locations of the top and bottom sides of each stud in the push load direction, which were 20 mm (Type A) or 45 mm (Type B) away from the steel flange surface. In addition, one uniaxial stirrup strain gauge (Fig. 6(b)) was mounted in each concrete slab for checking the status of concrete during the test process. The direction of these uniaxial strain gauges was along the stud shank or the stirrup.

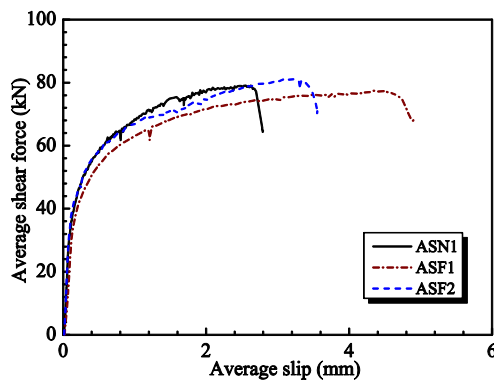## 3. Test results

3.1 Push-out failure mode

Fig. 7 presents the failure modes in the static and fatigue push-out tests. The stud root fracture and the surrounding concrete or SFRC damages were observed in all of the specimens. The images of the typical static concrete and SFRC damages and the stud root fracture were shown in Fig. 7(a). As to the fatigue failures, the images of the typical stud fractures were separately shown in Fig. 7(b), which contained three patterns: the stud root fracture (No. 1), the stud root fracture with the damages on the welding collar (No. 2), the stud root fracture with the damages on the welding collar and the base steel flange (No. 3). In addition, the concrete damage features in the fatigue tests were more or less similar to Fig. 7(a).
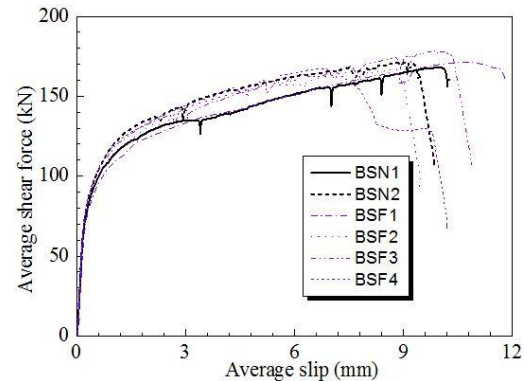
3.2 Static load-slip curves and strains

3.2.1 Static load-slip curves, stiffness and strength

Figs. 8(a) and (b) separately presents the load-slip curves derived from the static tests on the Type A and B push-out specimens. The average shear force denotes the shear force supported by one single stud in average, and the average slip denotes the average slip values monitored by the four slip sensors (Fig. 6(a)). According to the curves, the stud stiffness, the strength and the ultimate slip derived at the load maximum were summarized in Table 3. The influence of the SFRC on the stud stiffness, which was defined as the ratio of $P_u/3$ to the corresponding average

(a) The Type A push-out test results

(b) The Type B push-out test results

Fig. 8 Static load-slip curves

Table 3 Static test results and evaluations

| Specimen | Test | | | Eurocode4 | ASSHTO | JARA |
	Stiffness (kN/mm)	Strength (kN)	Ultimate slip (mm)	Strength (kN)	Strength (kN)	Strength (kN)
ASN1	379.1	79.1	2.62			63.2
ASF1	256.1	77.4	4.35	48.4	60.5	57.5
ASF2	397.2	81.3	3.33			64.5
BSN1	370.0	168.3	9.95	103.3		128.4
BSN2	383.2	170.9	8.94	103.3		128.4
BSF1	316.4	171.7	10.87	97.6		108.7
BSF2	395.2	165.5	8.66	97.6	129.1	108.7
BSF3	365.1	177.8	9.84	103.3		127.6
BSF4	412.0	168.0	6.63	103.3		127.6

(a) ASN1 & ASF1-2   (b) BSN1-2 & BSF1-2   (c) BSN1-2 & BSF3-4
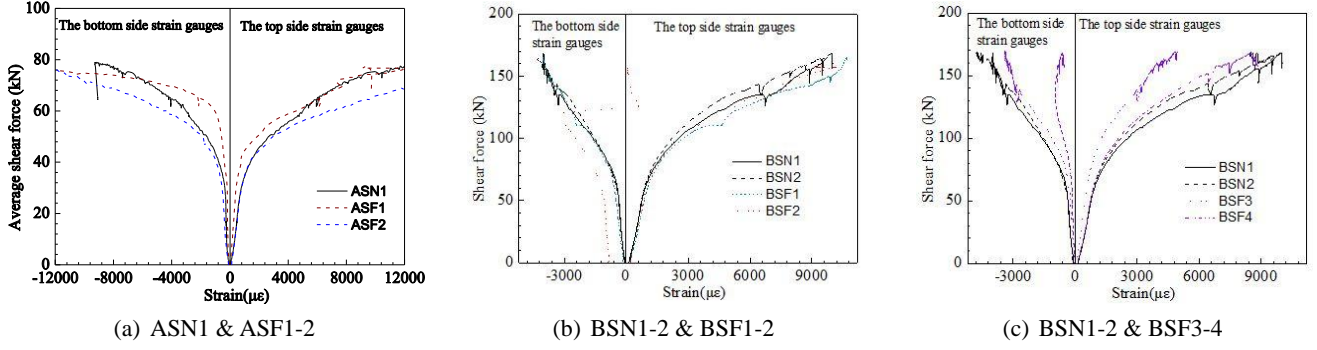
Fig. 9 Strains derived from the gauges mounted on the studs (Fig. 6(b))

slip, appeared to be not obvious. Meanwhile, its effect on the stud shear strength as listed was nearly the same as well. This is because the stud fracture was the main failure mode in all of the static tests. Concerning the ultimate slip in particular, it can be seen that the hardening stage in specimens with SFRC (ASF1 and ASF2) were longer, especially the ASF1 that had a larger volume percentage of steel fibers. However, the difference among the Type B specimens was not obvious.

Moreover, the test strength was compared with the evaluations based on AASHTO (2007), Eurocode 4 (CEN 2005), JARA (2012). Table 3 indicates that the static designs of stud in normal concrete and SFRC based on the above design codes are safe in general.

(1) AASHTO-LFRD (2007)

In AASHTO, the nominal stud shear resistance Q_n is expressed as Eq. (1), where A_{sc} is the stud cross section area; f'_c is the compressive strength of concrete for design; E_c is the elastic modulus of concrete and F_u is the stud tensile strength. For example, f'_c = 39.8 MPa E_c = 31500 MPa for normal concrete according to the material properties shown in Table 2, Meanwhile, according to the metal material test, F_u = 455.5 Mpa. Based on the Eq. (1), all of the static test specimens should have a failure mode governed by stud fracture, which is consistent with the test results. Moreover, the AASHTO was found to provide the highest evaluation results among all the specifications.

$$Q_n = 0.5 A_{sc}\sqrt{f'_c E_c} \leq A_{sc} F_u \tag{1}$$

(2) Eurocode 4 (CEN 2005)

In Eurocode 4, the design shear capacity of one stud P_{Rd} is expressed as Eq. (2), where γ_v is the partial factor and its value was set to 1.0 instead of the recommended 1.25 for comparison purposes; d is the shank diameter; f_u is the ultimate tensile strength of a stud; f_{ck} is the cylinder compressive strength of concrete; E_{cm} is the concrete modulus; and h_{sc} is the stud height. The value of α is determined by Eq. (3). For example, f_{ck} = 0.83×3.92 = 325 Mpa (based on ref. (Guo and Shi 2006)) E_{cm} = 35759 MPa for SFRC with 1.0% vol. fibers according to the material properties shown in Table 2. Based on the Eq. (2), all of the static test specimens should have a failure mode governed by stud fracture except BSF1 and BSF2 which were

supposed to be governed by the failure of SFRC. This is not fully consistent with the test results.

$$P_{Rd} = \frac{0.29\alpha d^2\sqrt{f_{ck}E_{cm}}}{\gamma_v} \leq \frac{0.8 f_u \pi d^2/4}{\gamma_v} \tag{2}$$

$$\begin{cases} \alpha = 0.2\left(\dfrac{h_{sc}}{d}+1\right) & \left(3 \leq h_{sc}/d \leq 4\right) \\ \alpha = 1 & \left(h_{sc}/d > 4\right) \end{cases} \tag{3}$$

(3) JARA (2012)

In the manual of road bridges of Japan (JARA 2012), the ultimate stud strength evaluation is expressed by the 6 times to the design allowable stud shear capacity Q_a as shown in Eq. (4), where d is the shank diameter; H is stud height; and σ_{ck} is the design strength of concrete. This equation indicates that the concrete district around the stud is critical to the allowable shear capacity of stud. σ_{ck} = 28.5 MPa for SFRC with 1.5% vol. fibers according to the material tests. The push-out failure mode cannot be reflected by this equation.

$$\begin{cases} Q_a = 9.4 d^2\sqrt{\sigma_{ck}} & \left(H/d \geq 5.5\right) \\ Q_a = 1.72 dH\sqrt{\sigma_{ck}} & \left(H/d < 5.5\right) \end{cases} \tag{4}$$

3.2.2 Static strains of stud

The relationship between the measured average stud strain and the static shear force was shown in Fig. 9. Generally, the top side was in tension and the bottom side was in compression. And the compressive strain appeared to be smaller than the tensile strain because of the axial tensile action on stud. In Fig. 9(a), the stud strains of ASF1 were smaller than those of ASN1 until approaching the ultimate loading stage. The higher strength and modulus of SFRC as listed in Table 2 contributed by the steel fibers in ASF1 may be the main reason. This also explained that the stud strains of BSF3 and BSF4 appeared to be smaller than the BSN1 and BSN2 (Fig. 9(c)). On the other side, the stud strains of the ASF2 (Fig. 9(a)) which had the relatively lower concrete compressive strength and modulus appeared to be larger than those of ASN1. Likewise, the stud strains of BSF1 and BSF2 were also slightly larger than the BSN1 and BSN2 (Fig. 9(b)).

Table 4 Fatigue test results

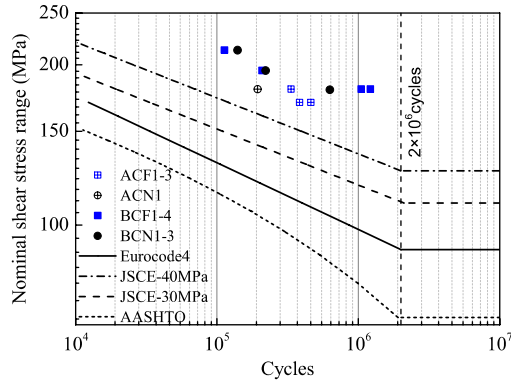| Specimens	Concrete	Load range (P_u)	Stress range (MPa)	Fatigue life cycles
ACN1	Normal	0.32	180	193800
ACF1	SFRC (1.0%)			334065
ACF2	SFRC (1.0%)	0.30	170	460792
ACF3	SFRC (0.5%)			383375
BCN1	Normal	0.36	213	142416
BCF1	SFRC (1.5%)			113042
BCN2	Normal	0.33	195	221077
BCF2	SFRC (1.5%)			208386
BCN3	Normal	0.30	180	630018
BCF3	SFRC (1.5%)			1048019
BCF4	SFRC (1.0%)			1216796

Fig. 10 Fatigue test results and specification-based S-N curves

3.3 Cyclic features

3.3.1 Fatigue life and discussion

The stud fatigue lives in the tests were summarized in Table 4. It can be seen that the stud fatigue life in both of the Type A and Type B specimens at the 180 MPa shear stress range appeared to be obviously higher when the stud was embedded into the SFRC. Moreover, concerning the Type A specimens with the 170 MPa shear stress range, the stud fatigue life of ACF2 which had a larger steel fiber volume percentage was higher than that of ACF3. However, concerning the Type B specimens which had the cyclic shear stress range larger than 180 MPa, the stud fatigue life was not influenced by the SFRC so significantly.

Furthermore, the test results of fatigue life was shown in Fig. 10 together with the fatigue S-N curves of AASHTO (2007), Eurocode 4 (CEN 2005) and JSCE (2007). Although all of the design codes can guarantee the safe fatigue design of stud in both of the normal concrete and the SFRC, the safety redundancies of some specification-based S-N curves appear unnecessary large such as the S-N curve of AASHTO. On the other hand, the JSCE S-N curve is close to the test results. It can make the fatigue design of stud more economical but the safety redundancy becomes small.

(1) AASHTO-LFRD (2007)

In AASHTO, the corresponding stud fatigue life evaluation equation is shown in Eq. (5). N_R is the fatigue life cycles; $\Delta\tau_R$ is the stud shear stress range. This equation only concerns the effect of stress range on stud fatigue performance.

$$\Delta\tau_R = 4\alpha/\pi = 303 - 37.6\log N_R \qquad (5)$$

(2) Eurocode 4 (CEN 2005)

In Eurocode 4, the fatigue life evaluation equation for one stud in normal concrete is shown in Eq. (6). N_R is the fatigue life cycles; $\Delta\tau_R$ is the stud shear stress range; m is the slope of the fatigue strength curve with the value $m=8$. The coefficient a can be derived from Eq. (7). $N_c = 2000000$; $\Delta\tau_c = 90$ MPa, which corresponds to 2000000 load cycles. Like the Eq. (5), the Eq. (6) only considers the effect of stress range on stud fatigue life as well.

$$\log N_R = a - m\log\Delta\tau_R \qquad (6)$$

$$a = \log N_c \Delta\tau_c^{\ m} \qquad (7)$$

(3) JSCE (2007)

In the Japanese Standard Specification for Hybrid Structure (2007), effects of concrete strength, stud flexibility and concrete casting direction on one stud fatigue life are quantified. The evaluation is specified in Eq. (8) and (9) for the concrete casted in the beam direction. V_{ssrd} is the cyclic shear load range; V_{ssuo} is specified in Eq. (9); A_{ss} is the cross-sectional area of stud shank; f'_{cd} is about the concrete compressive strength; h_{ss} and d_{ss} are the stud shank height and diameter, respectively; γ_b is a coefficient with the recommended value of 1.0.

$$V_{ssrd}/V_{ssuo} = 0.99N^{-0.105} \qquad (8)$$

$$V_{ssuo} = \left(31A_{ss}\sqrt{(h_{ss}/d_{ss})f'_{cd}} + 10000\right)/\gamma_b \qquad (9)$$

3.3.2 Stiffness degradation, cyclic slip and strain

The fatigue induced stud shear stiffness degradations were summarized in Fig. 11. Due to the data insufficiency, the ACF2 and ACF3 were not included. The residual stiffness ratio in the vertical axis means the ratio of the fatigue residual stiffness to the initial static stiffness. It can be seen that the stud shear stiffness dropped to nearly half or even less during the early period of load cycles in general. The interlayer bonding failure and the local concrete damage near the stud root may be the reasons. Moreover, the effect of SFRC on the stud degradation was not obvious according to Fig. 11(b), when the stud shear stress range was larger than 180 MPa. However, Fig. 11(a) and Fig. 11(c) show that the stud residual stiffness ratio of the specimens with SFRC appeared to be larger and dropped relatively slower than the specimens with the normal concrete when the stud shear stress range was 180 MPa.

The development of the interlayer cyclic slip ranges were shown in Fig. 12. They kept stable until the late periods of the stud fatigue lives. Fig. 12(a) shows the comparison between ACN1 and ACF1, the cyclic slip range developed more slowly in ACF1 with the SFRC. Similar situation could be found in Fig. 12(c) as well, showing the comparison among BCN3, BCF3 and BCF4. On the other hand, Fig. 12(b) shows the comparison between BCN2 and BCF2 which were with the cyclic stud shear stress range larger than 180 MPa. It can be seen the effect of SFRC is not significant.

Fig. 13 summarized the cyclic tensile strain range development at the top side of stud as introduced in Fig. 6(b). It can be seen in general the stud strain developed
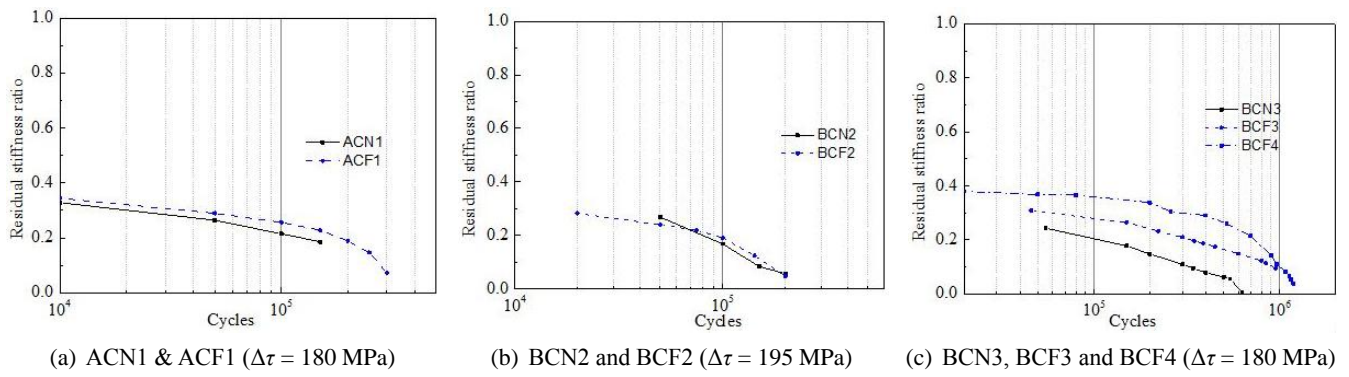

(a) ACN1 & ACF1 ($\Delta\tau$ = 180 MPa) (b) BCN2 and BCF2 ($\Delta\tau$ = 195 MPa) (c) BCN3, BCF3 and BCF4 ($\Delta\tau$ = 180 MPa)

Fig. 11 Stud shear stiffness degradation with fatigue load cycles

(a) ACN1 & ACF1 ($\Delta\tau$ = 180 MPa) (b) BCN2 and BCF2 ($\Delta\tau$ = 195 MPa) (c) BCN3, BCF3 and BCF4 ($\Delta\tau$ = 180 MPa)
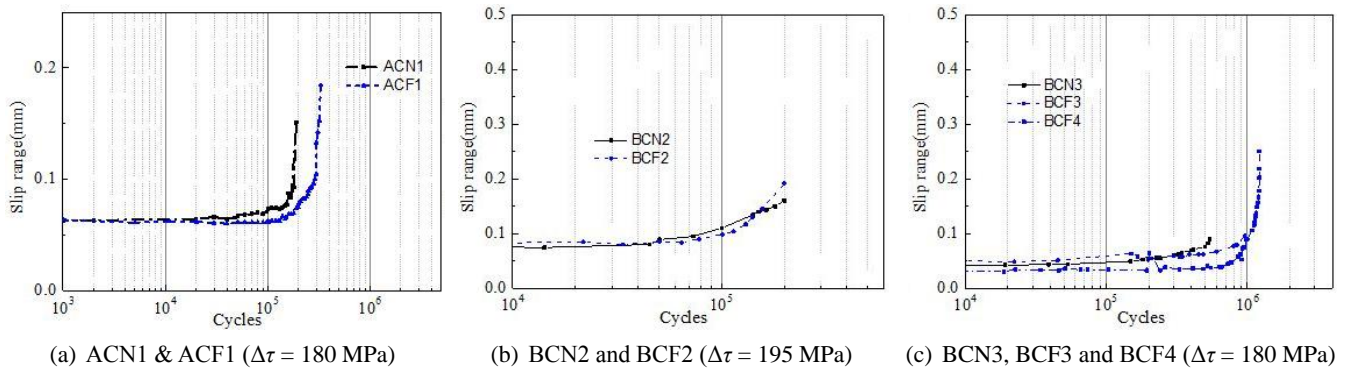
Fig. 12 Development of the cyclic slip range with the fatigue load cycles

(a) ACN1 & ACF1 ($\Delta\tau$ = 180 MPa) (b) BCN2 and BCF2 ($\Delta\tau$ = 195 MPa) (c) BCN3, BCF3 and BCF4 ($\Delta\tau$ = 180 MPa)
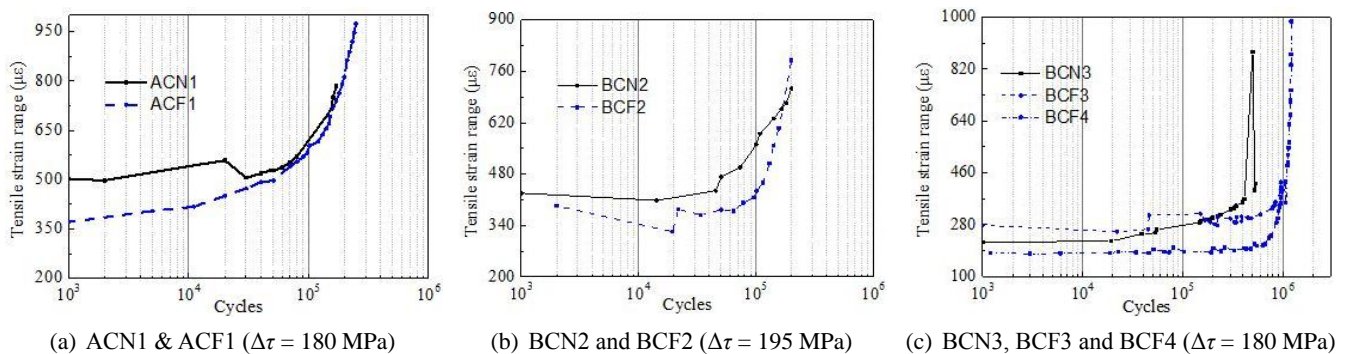
Fig. 13 Development of the cyclic tensile strain range of stud with the fatigue load cycles

relatively slower in the specimen with SFRC.

The observations on the interlayer slips and the stud strains indicated that the steel fibers in concrete may have a favorable effect on the stud fatigue performance. According to the test results as introduced, such effect was particularly obvious when the cyclic stud shear stress range was not larger than 180 MPa.

4. Analytical discussion

4.1 Model setup

The effect of SFRC on the stud performance was also discussed through the static and fatigue analysis by ABAQUS. The analysis model was shown in Fig. 14, which

was a quarter part of the Type B test specimen. This was in terms of the symmetric feature. The C3D8R solid element was used to simulate the concrete, studs and steel plates. The T3D2 truss element was used to simulate the steel bars. The load area was the same to the test specimens. The bonding and friction behavior of the steel-concrete and the stud-concrete interlayers were simulated by the exponential decay friction models in the contact algorithm (Abaqus Documentation 2014), including the static and kinematic phases.

As listed in Table 5, there were 8 models in the analysis. Concerning the fatigue analysis in particular, 4 load cycles were introduced, which were actually composed by 90 static load steps. And there were two kinds of fatigue load patterns ($\Delta\tau$ = 213 MPa and 180 MPa) respectively applied in the load cycles. In terms of the tensile strength values,
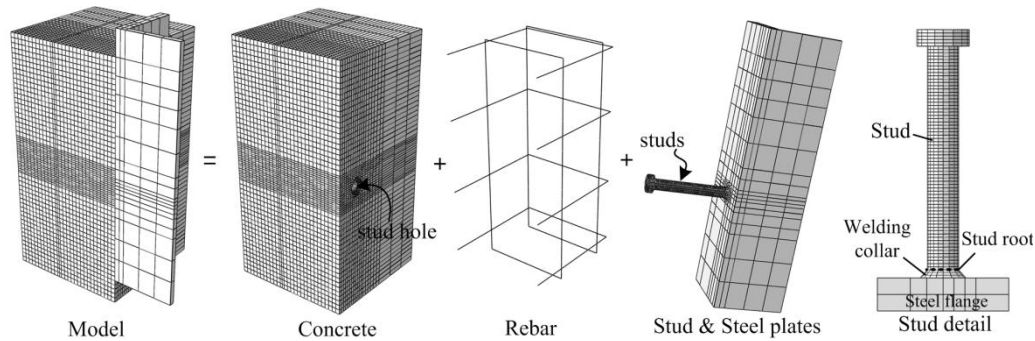

Fig. 14 FEM analysis model based on Type B push-out test specimen (stud shank diameter: 19 mm, stud height: 150 mm)

Table 5 The FEM models for the static and fatigue analysis

Models	Analysis type	Concrete type	f_c (MPa)	f_t (MPa)	Cyclic stress range
SNA1		concrete1	39	3.0	-
SNA2	Static	concrete2	30	2.0	-
SFA1		SFRC1	39	3.5	-
SFA2		SFRC2	30	2.3	-
CNA1		concrete1	39	3.0	213
CNA2	Fatigue	concrete1	39	3.0	180
CFA1		SFRC1	39	3.5	213
CFA2		SFRC1	39	3.5	180

(a) Concrete compression   (b) Concrete tension   (c) Non-concrete materials
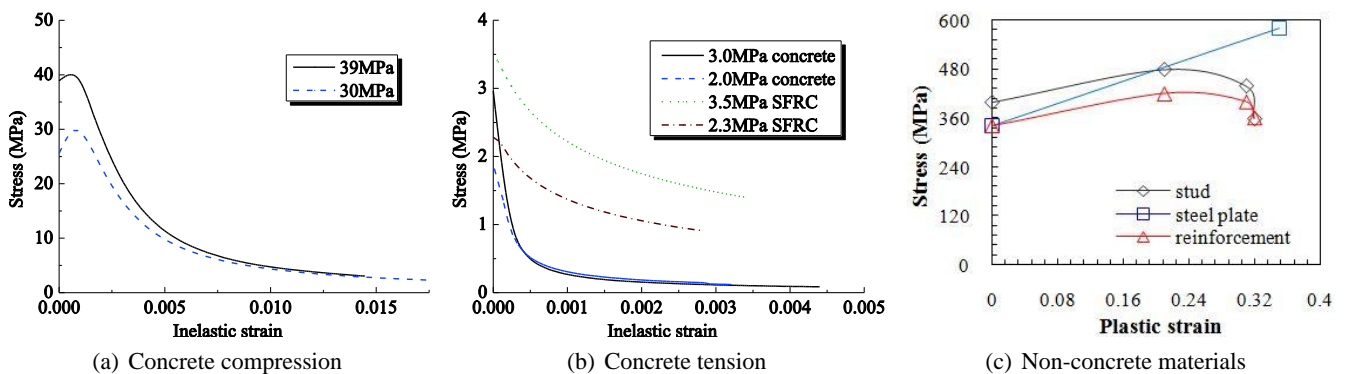
Fig. 15 Uniaxial material constitutive laws

(a) Compression   (b) Tension
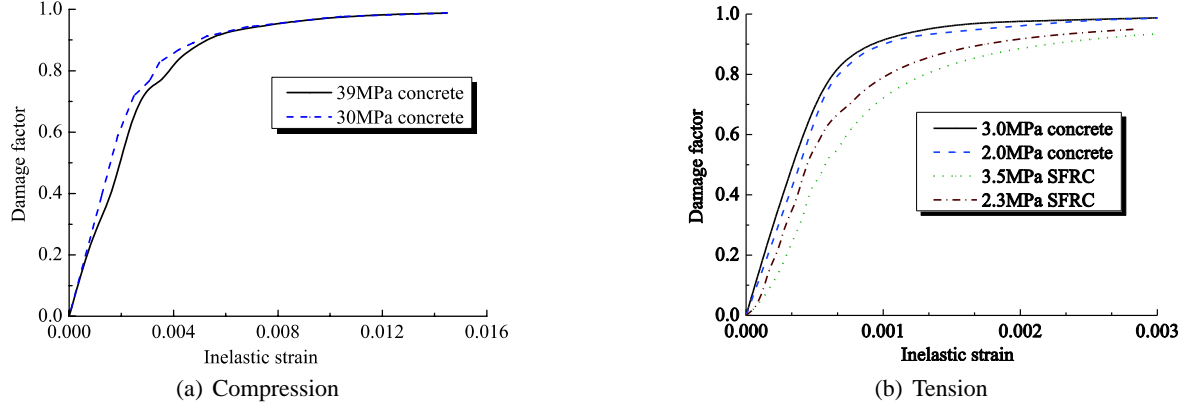
Fig. 16 Uniaixal concrete damage models (damage factor 0: intact; 1: full damage)

(a) Concrete and SFRC damage distributions (0: Intact; 1: full damage)   (b) Stud solid element (C3D8R) stiffness degradation distributions (0: intact; 1: 100% degradation)
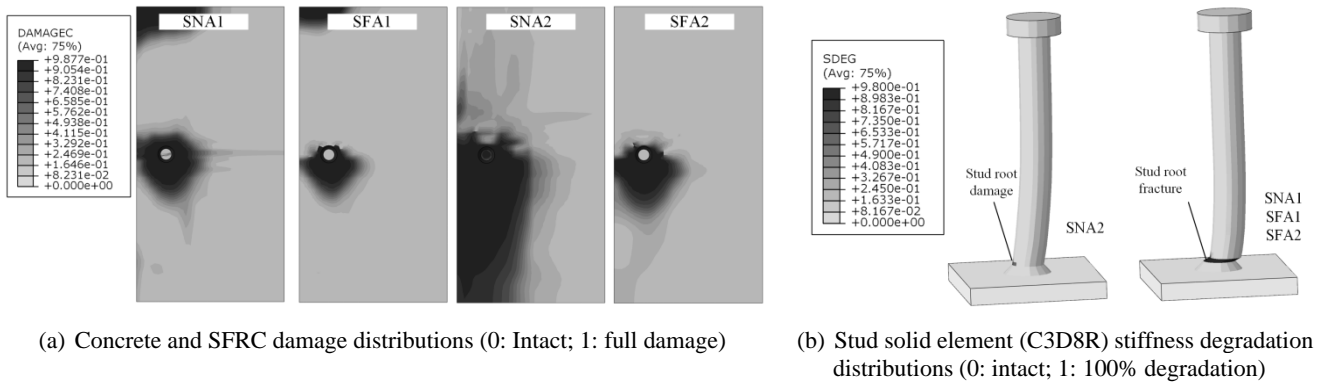
Fig. 17 Analyzed failure modes

there were 4 types of concrete (Concrete 1, 2, SFRC 1, 2 in Table 5) used in the analysis. Compared with the normal concrete, the tensile strength of SFRC was assumed to be 15% higher based on the material test results summarized in Table 2. The concrete compressive strength had two values which were 39 and 30 MPa (low strength). And the modulus was set to be constant in these models.

The detail concrete stress-inelastic strain (σ-ε_{in}) relationships as shown in Figs. 15(a) and (b) were based on the material tests (for 39 MPa concrete) and assumptions. In particular, the tensile behavior of SFRC summarized in Fig. 15(b) were governed by Eq. (10) (MOHURD 2002) where f_t are the uniaxial tensile strength of concrete; ε_t are the strains tensile peak stresses; α_t are regression parameters, the specific f_t, ε_t and ε_t values of SFRC 1 and 2 as listed in Table 6 were 3.5 MPa, 1560 $\mu\varepsilon$, 0.15 and 2.3 MPa, 1640 $\mu\varepsilon$, 0.15. In addition, the inelastic strain ε_{in} is expressed by Eq. (11) (Abaqus Documentation 2014) where E is the initial elastic modulus. According to Fig. 15(b), the tensile unloading of SFRC was much slower than that of normal concrete. The non-concrete material constitutions were shown in Fig. 15(c).

$$\sigma = \begin{cases} f_t\left[1.2\left(\varepsilon/\varepsilon_t\right)-0.2\left(\varepsilon/\varepsilon_t\right)^6\right] & , \ \varepsilon/\varepsilon_t \leq 1 \\ f_t\,\varepsilon/\varepsilon_t\left[\alpha_t\left(\varepsilon/\varepsilon_t\right)^{1.7}+\varepsilon/\varepsilon_t\right] & , \ \varepsilon/\varepsilon_t > 1 \end{cases} \quad (10)$$

In addition, the assumed damage plasticity models of the

concrete and the stud were introduced by referencing Xu *et al.* (2012)'s analysis approach. These models were used for analyzing the failure modes and the fatigue damage accumulations. Fig. 16 shows the damage models of concrete. It can be seen the damage evolution of SFRC was lower than the concrete. For the damage evolution of stud, an exponential correlation between the damage variable D and the plastic displacement was established based on Abaqus Documentation (2014). The exponential law parameter was 0.01 and the equivalent plastic displacement was related to dimension size of discrete elements.

4.2 Static analysis

The analyzed static failure modes were summarized in Figs. 17(a) and (b). The local concrete damage near the stud roots can be observed according to the damage distributions shown in Fig. 17(a). These were consistent with the test failure mode as shown in Fig. 7. Further it can be found that the SFRC restrained the damage area based on the concrete/SFRC damage distribution comparison between SNA1 and SFA1. And such phenomenon appeared to be much more significant regarding to the comparison between SNA2 and SFA2 of which the concrete compressive strength was lowered down to 30 MPa. Concerning the stud itself shown in Fig. 17(b), the degradation mainly appeared near the stud root. In general, the failure mode in SNA1 and SFA1 were dominated by the stud root fracture according to the element stiffness degradation distributions. And the
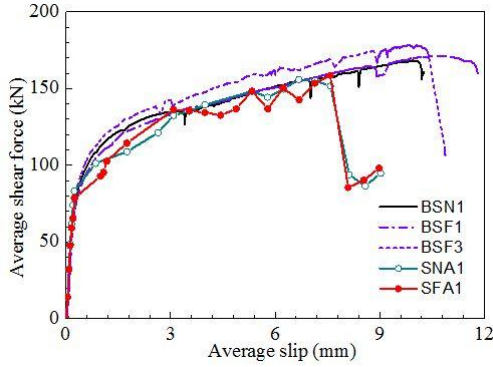
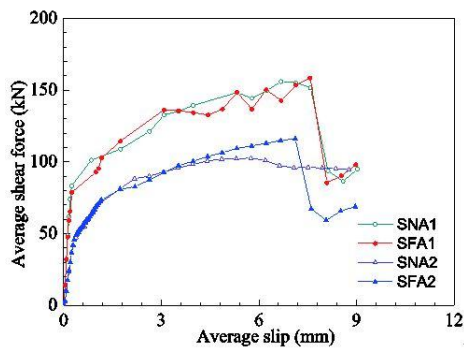Fig. 18 Load-slip curves in push-out tests and simulations

Fig. 19 The analyzed load-slip curves

failure mode of SNA2 appeared to be the concrete crush due to the low concrete compressive strength. However the SFRC in SFA2 significantly restrained the crush, transforming the main failure mode to the stud fracture.

Fig. 18 shows the static load-slip comparison between the test and analysis results. They agreed with each other in general, showing that the effect of SFRC on the stud shear stiffness and strength was not obvious. But this was in condition that the concrete was 39 MPa, making the push-out failure mode dominated by the stud fracture (Fig. 17). In case that the concrete was relatively weak, leading to a concrete crush failure mode like SNA2, the situation tended to be different in terms of Fig. 19. It can be seen that the favorable tensile performance of SFRC increased the stud shear strength obviously in SFA2 as compared with SNA2. This is because that the SFRC restrained the crush extent in SFA2 and transformed the failure mode from the concrete crush to the stud fracture (Fig. 17).

4.3 Fatigue analysis

Furthermore, the analyzed maximum principal strain distributions along the stud root section edge (Fig. 14) at the cyclic load peak and valley were summarized in Fig. 20. The 0 degree position corresponds to the top point of stud root section in the push load direction and the180 degree position corresponds to the bottom point. It shows that the strain maximum and the cyclic strain range maximum both appeared at the bottom point, and they were both tensile strains.
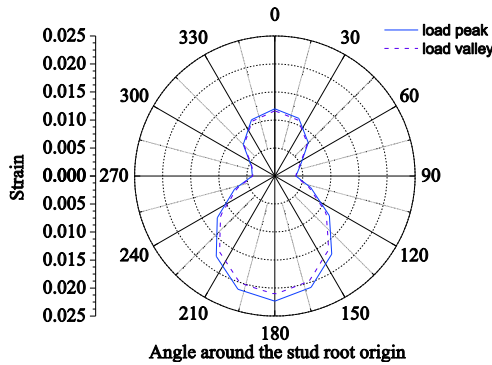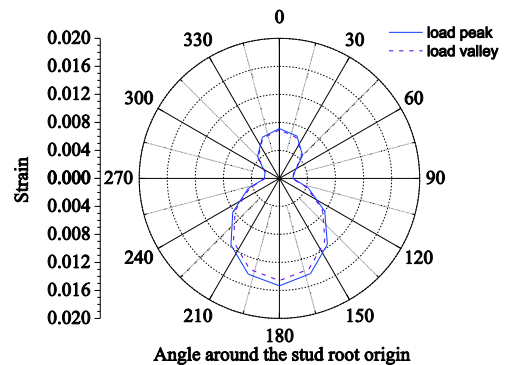

(a) CNA1 ($\Delta\tau$ = 213 MPa)
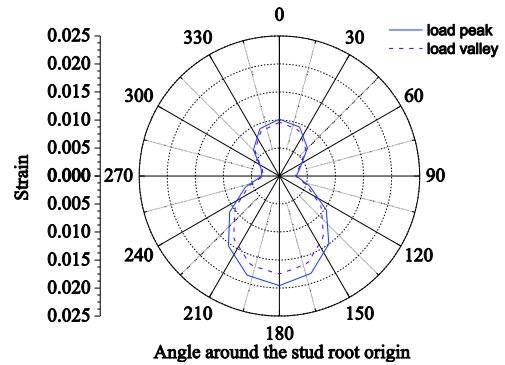
(b) CFA1 ($\Delta\tau$ = 213 MPa)
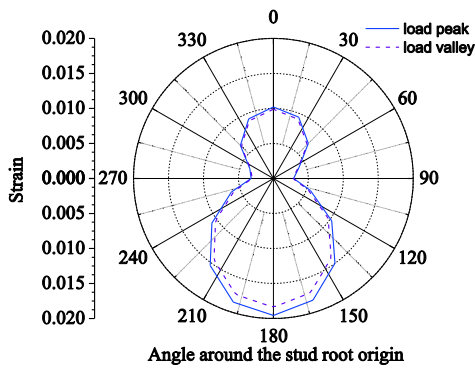
(c) CNA2 ($\Delta\tau$ = 180 MPa)

(d) CFA2 ($\Delta\tau$ = 180 MPa)

Fig. 20 The maximum principal strain distribution around stud root section edge (Fig. 14)
(0 degree: top side of stud; 180 degree: bottom side of stud in the push load direction)
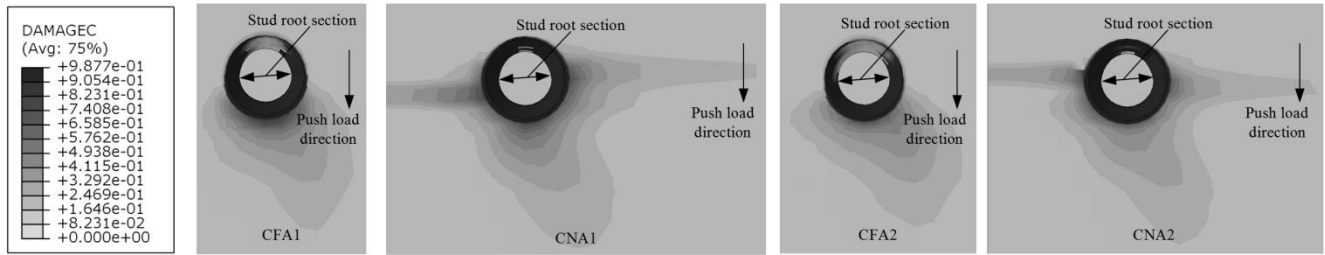
Fig. 21 Analyzed accumulated fatigue damage distributions on the concrete or SFRC surrounding the stud roots (0: Intact; 1: full damage)

When the cyclic shear stress range was 213 MPa in CNA1 (Fig. 20(a)) and CFA1 (Fig. 20(b)), the effect of SFRC on the strain distribution was not significant in terms of the comparison between them. The cyclic strain range of CFA1 was smaller than that of CNA1, respectively 0.00122 and 0.00202. But the strain maximums at the cyclic load peak were respectively 0.022330 and 0.019570. On the other hand, when the cyclic shear stress range was 180 MPa, it can be found that the SFRC lowered down the cyclic strain range and the strain maximum according to Figs. 20(c) and (d). The cyclic strain ranges of CNA2 and CFA2 were 0.00118 and 0.00074, and the strain maximums were respectively 0.01956 and 0.01534. These were consistent with the test observations that the SFRC helped to improve the stud fatigue life in condition that the cyclic stud shear stress range was not larger than 180MPa. In another perspective, this actually confirmed that the good tensile performance of SFRC could be favorable to the stud fatigue behavior.

On the other side, the analyzed 4 load cycles concrete and SFRC fatigue damage accumulations near the stud roots were shown in Fig. 21. It can be seen the damage areas of CFA1 and CFA2 were smaller than those of CNA1 and CNA2. This shows the effect of SFRC on restraining the fatigue damage accumulation. Concerning the severe damage districts in the circle around the stud root section in particular, it can be seen the difference between CFA2 and CNA2 seems to be more obvious than that between CFA1 and CNA1. In other words, such effect of SFRC on restraining the fatigue damage accumulation might be more effective when the fatigue load range was small.

5. Conclusions

The mechanical performance of the stud shear connector in the steel fiber reinforced concrete (SFRC) was investigated and discussed by the push-out tests and analysis. The summations were listed as follows.

(1) The failure modes in the static and fatigue push-out tests both consisted of the stud fractures and the crushes of the surrounding concrete or SFRC. Particularly, there were three types of fatigue induced stud fractures found in the tests, which were the stud root fracture, the stud root fracture with the welding collar damage and the stud root fracture with the damages on the welding collar and flange.

(2) According to the static push-out test results, the

effect of SFRC on the stud shear stiffness and strength was not obvious. But this was in condition that the test failure mode mainly appeared as the stud fracture. When the concrete compressive strength was changed to be relatively low in the analysis discussion, leading to a concrete crush failure mode, the SFRC was found to have a favorable effect of restraining concrete damage development and improving the stud shear strength. Moreover, the static designs of stud in the SFRC according to the design codes of AASHTO, Eurocode 4 and JARA were confirmed to be safe in general.

(3) According to the fatigue push-out test results, the SFRC helped to improve the stud fatigue performance when the cyclic stud shear stress range was not larger than 180MPa. According to the analysis, the favorable tensile performance of SFRC can lower down the maximum principal strain level around the stud root and thus release the concrete fatigue damage accumulation, especially when the stress range was not larger than 180MPa.

(4) Based on the comparison between the stud fatigue lives in the tests and the S-N curves in the design codes, the fatigue life estimation of Eurocode 4 appeared to be less conservative than that of AASHTO, and to have higher safety redundancy than that of JSCE Hybrid Structure Guidelines. As to the specific fatigue strength of stud in SFRC, the current specimen amount is not enough. Thus it needs a further study.

Acknowledgments

References

AASHTO (2007), Bridge design specifications; AASHTO-LFRD, American Association of State Highway and Transportation Officials, USA.

ABAQUS Documentation (2014), Version 6.13, Dassault System, USA.

Badie, S.S., Morgan, G.A.F., Tadros, M.K. and Sriboonma, K. (2011), "Full-scale testing for composite slab/beam systems made with extended stud spacing", *J. Bridge Eng*., *ASCE*, **16**(5), 653-661.

Eurocode 4 (2005), Design of Composite Steel and Concrete Structures. Part 2 General Rules and Rules for Bridges; European Committee for Standardization, BS EN 1994-2:2005; Brussels, Belgium.

Cui, Y. and Nakashima, M. (2012), "Application of headed studs in steel fiber reinforced cementitious composite slab of steel beam-column connection", *Earthq. Eng. Eng. Vib*., **11**(1), 11-21.

Choi, J., Yamaguchi, K., Hino, S. and Kajihara, H. (2011), "Strength characteristic and shear evaluation of perfobond rib of super light weight concrete with steel fiber", *J. Struct. Eng*., *JSCE*, **57A**, 1007-1016. [In Japanese]

Gao, Y.M., Zhou, Z.X., Liu, D. and Wang, Y.H. (2016), "Cracking of a prefabricated steel truss-concrete composite beam with pre-embedded shear studs under hogging moment", *Steel Compos. Struct*., *Int. J*., **21**(5), 981-997.

Guo, Z.H. and Shi, X.D. (2006), *Reinforced Concrete Theory and Analysis*, Tsinghua University Press, Beijing, China, pp. 13-14. [In Chinese]

Hosaka, T., Yamada, T. and Nakano, M. (2000), "Continuous composite railway bridge using steel fiber reinforced lightweight concrete (Asa Monobekawa Bridge)", *Concrete Eng*., *JSCE*, **38**(6). [In Japanese]

Japan Road Association (JARA) (2012), Manual of Road Bridges (Steel Bridges); Committee on Steel Structures, Japan. [In Japanese]

Japan Society of Civil Engineers (JSCE) (2007), Guidelines for Performance Verification of Steel-concrete Hybrid Structures; Committee of Steel Structure, Japan.

Japan Society of Steel Construction (JSSC) (1996), Push-out Test for Headed Stud and Related Research on Stud (draft); JSSC Technical Rep. 35, Japan. [In Japanese]

Ju, X.C. and Zeng, Z.B. (2015), "Study on uplift performance of stud connector in steel-concrete composite structures", *Steel Compos.Struct*., *Int. J*., **18**(5), 1279-1290.

Lam, D. and Nip, T.F. (2002), "Effects of steel fibers reinforcement on shear studs capacity of composite beams", Technical Report; School of Civil Engineering, University of Leed, UK.

Lin, W.W., Yoda, T. and Taniguchi, N. (2014), "Application of SFRC in steel-concrete composite beams subjected to hogging moment", *J. Constr. Steel Res*., **101**, 175-183.

Lin, Z.F., Liu, Y.Q. and He, J. (2015), "Static behaviour of lying multi-stud connectors in cable-pylon anchorage zone", *Steel Compos. Struct*., *Int. J*., **18**(6), 1369-1389.

Luo Y.B., Hoki K., Hayashi K. and Nakashima M. (2016), "Behavior and strength of headed stud-SFRCC shear connection: 1 experimental study", *J. Struct. Eng*., *ASCE*, **142**(2).

Mirza, O. and Uy, B. (2009), "Effects of steel fibre reinforcement on the behavior of headed stud shear connectors for composite steel-concrete beams", *Adv. Steel Constr*., **5**(1), 72-95.

Ministry of Housing and Urban-Rural Development of China (MOHURD) (2002), Code for Design of Concrete Structures GB50010-2002; Beijing, China. [In Chinese]

Nguyen, G.B. and Machacek, J. (2016), "Effect of local small diameter stud connectors on behavior of partially encased composite beams", *Steel Compos. Struct*., *Int. J*., **20**(2), 251-266.

Public Works Research Institute (PWRI) (2009), Design and Constructional Manual of Steel Bridge Deck Reinforcement by Using SFRC; Research Report and Guidelines, October, Japan.

[In Japanese]

Shim, C.S., Lee, P.G., Kim, D.W. and Chuang, C.H. (2008), "Effects of group arrangement on the ultimate strength of stud shear connection", *Proceedings of International Conference on Composite Construction in Steel and Concrete*, *Composite Construction in Steel and Concrete VI*, ASCE, Tabernash, CO, USA, July, pp. 92-101.

Xu, C. and Sugiura, K. (2013), "Parametric push-out analysis on group studs shear connector under effect of bending-induced concrete cracks", *J. Constr. Steel Res*., **89**, 86-97.

Xu, C., Sugiura, K., Wu, C. and Su, Q.T. (2012), "Parametrical static analysis on group studs with typical push-out tests", *J. Constr. Steel Res*., **72**, 84-96.

DL